J Mater Sci (2018) 53:5216–5228

Energy materials

A strategy to boost electrochemical properties of the graphene oxide–poly(3,4-ethylenedioxythiophene) composites for supercapacitor electrodes

Haihan Zhou[1,*], Xiaomin Zhi[1], and Hua-Jin Zhai[1,*]

[1] *Institute of Molecular Science, Key Laboratory of Materials for Energy Conversion and Storage of Shanxi Province, Key Laboratory of Chemical Biology and Molecular Engineering of Education Ministry, Shanxi University, Taiyuan 030006, China*

Received: 7 November 2017
Accepted: 6 December 2017
Published online: 18 December 2017

ABSTRACT

We report on a strategy to enhance electrochemical capacitive properties of the graphene oxide–poly(3,4-ethylenedioxythiophene) (GO-PEDOT) composites. The basic idea is to convert GO to carboxylated GO (CGO) via carboxylation treatment. Composite electrodes of CGO-doped PEDOT (CGO-PEDOT) are fabricated by in situ electrochemical polymerization, which make adequate use of oxygenated groups on the basal plane of CGO to combine with PEDOT for enhanced supercapacitive properties. During carboxylation, hydroxyl and epoxide groups on GO are converted to carboxyl groups, as characterized by X-ray photoelectron spectroscopy and Fourier transform infrared spectroscopy. Electrochemical measurements show that CGO-PEDOT electrodes have boosted supercapacitive performances as compared to GO-PEDOT. In CGO nanosheets, the edges and basal planes are both covered with carboxyl groups, providing more active sites for combination with PEDOT coating, in contrast to GO nanosheets that only use edged carboxyl groups. The as-prepared CGO-PEDOT composite electrodes exhibit superior rate capability, high areal specific capacitance (90.9 mF cm^{-2} at 10 mV s^{-1}), and excellent cycling stability (retaining 99.6% of initial capacitance for 5000 cycles). This work is anticipated to stimulate further research interest for CGO-based composite electrodes in electrochemical energy storage.

Introduction

Graphene is a two-dimensional nanomaterial of one-atom-thick carbon. Since the discovery in 2004, graphene has been widely investigated in a diversity of technological applications including nanoelectronics, sensors, bioelectrodes, touch control display, and electrochemical energy storage due to its outstanding properties [1–5]. As a class of energy storage devices, supercapacitors (SCs) have received significant

Address correspondence to E-mail: hhzhou@sxu.edu.cn; hj.zhai@sxu.edu.cn

https://doi.org/10.1007/s10853-017-1904-x

attention. They have greater power density and longer cycling stability than secondary batteries, as well as higher energy density than conventional capacitors. SCs are anticipated for applications in wearable electronics, electric and hybrid vehicles, and energy harvesting [6–8]. Among various electrode materials used for SCs, graphene has become the most promising owing to its high specific surface area, superb chemical stability, ideal electrical conductivity, and good mechanical strength [9, 10].

Graphene oxide (GO) possesses abundant oxygen-containing functional groups on their basal planes and edges: epoxide, hydroxyl, carbonyl, and carboxyl groups. GO as a single sheet of graphite oxide has large specific surface area and high water compatibility [11, 12]. It can be directly prepared in large quantities from graphite and has emerged as the most common starting material for graphene-based applications. GO is promising for use in composites with other materials, and its tunable oxygen-containing functional groups benefit surface modification [13, 14]. Among π-conjugated conducting polymers (CPs), PEDOT has been extensively studied as supercapacitor electrode materials because of high electrical conductivity, fast charge/discharge kinetics, wide potential window, and environmental compatibility [15]. However, a drawback of poor cycle life restricts its application in supercapacitors. Charge storage in PEDOT is realized by fast doping/dedoping of counter anions into polymer chains, while swelling and shrinkage take place, causing considerable volume changes in charging/discharging. The volume change eventually results in electrode degradation during cycling [16, 17]. To overcome this, hybrid electrode materials have been explored by compositing PEDOT with mechanically strong carbon materials, which provide extra mechanical support and allow space for volume swelling and shrinkage [18, 19].

Recently, much attention has been paid for the GO-PEDOT composites as supercapacitor electrode materials. In the studies [20–25], GO-PEDOT composites show acceptable electrical conductivity despite the fact that GO is insulating, which is probably caused by π–π interaction between thiophene rings and GO layers. The composites have prolonged cycle life. Hydrophilic GO also increases wettability of the composites, promoting their performances in aqueous electrolytes. To date, GO-PEDOT composites were primarily prepared by in situ electrochemical polymerization, in which electroactive substances can directly grow on the current collector without mixing with binders and additives. During electropolymerization of PEDOT, negatively charged GO acts not only as a weak electrolyte, but also as a charge-balancing dopant. Thereinto, the anionic nature of GO mainly originates from ionization of carboxyl groups. In other words, carboxyl groups on GO nanosheets provide active sites for PEDOT nucleation. However, GO has quantities of hydroxyl and epoxy groups at the basal planes, in addition to lesser carboxyl groups on edges of nanosheets [26]. Therefore, the fact that GO-PEDOT composites only utilize edged carboxyl groups to bind PEDOT leaves the ample oxygenated groups on the basal planes intact. This also means that polymerized PEDOT aggregates on the edges of GO rather than being dispersed on the basal planes, as illustrated in Fig. 1. To make full use of oxygen-containing sites on the basal planes of GO sheets and to load more PEDOT, we put forward a strategy of converting hydroxyl and epoxy groups on the basal planes of GO to carboxyl groups via carboxylation treatment.

In this contribution, we allow GO to suffer from carboxylation and obtain carboxylated GO (CGO), that is, all-round carboxyl-covered graphene sheets with edged and basal oxygen-containing sites. CGO offers more and dispersed active sites for PEDOT polymerization, which facilitate the formation of a stable, uniform, and orderly composite. CGO-PEDOT and GO-PEDOT composites were fabricated by in situ electrochemical polymerization. Their compositions and morphologies were characterized by Fourier transform infrared spectroscopy (FTIR), X-ray diffraction (XRD), energy-dispersive X-ray spectroscopy (EDS), scanning electron microscope (SEM), and transmission electron microscopy (TEM). Electrochemical capacitive properties were investigated and compared using cyclic voltammetry (CV), galvanostatic charge/discharge (GCD) tests, and electrochemical impedance spectroscopy (EIS). The results show that CGO-PEDOT electrodes have boosted supercapacitive performances with respect to GO-PEDOT.

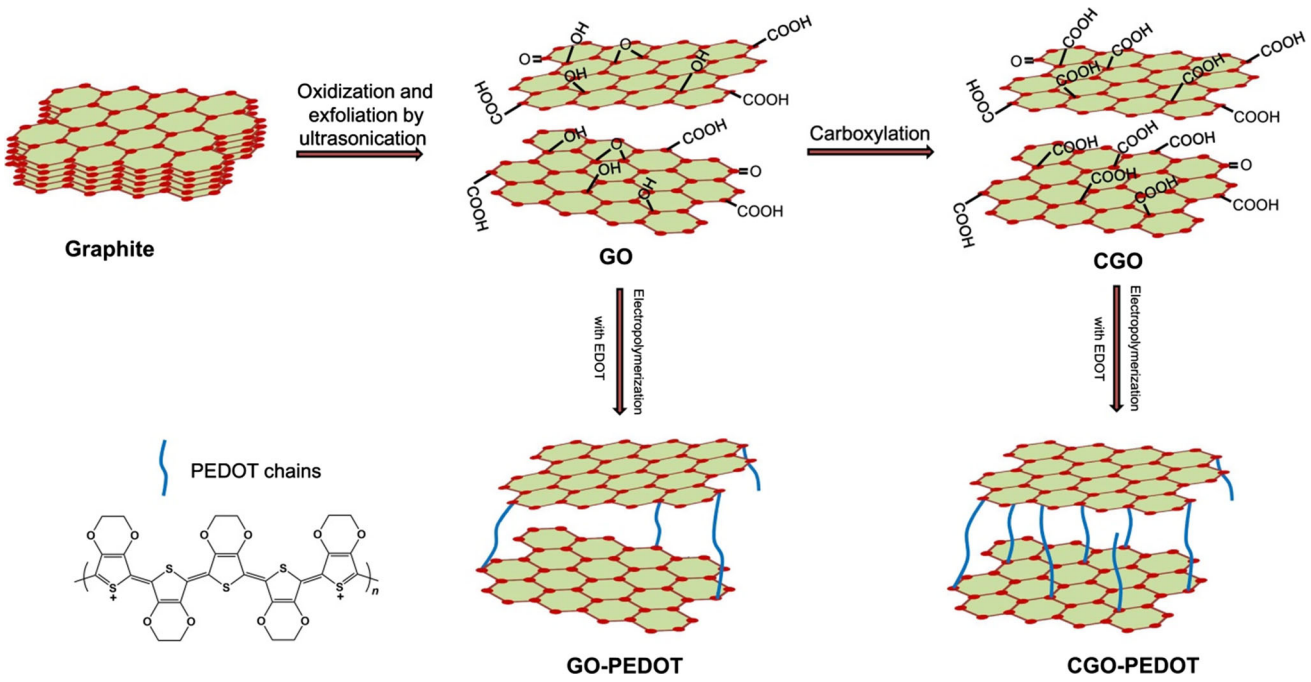

Figure 1 Schematic of the preparation procedures of GO, CGO, GO-PEDOT, and CGO-PEDOT.

Experimental section

Preparations of GO and CGO

As shown in Fig. 1, GO was obtained from graphite powder on the basis of a modified Hummers method [27, 28]. Briefly, 3.0 g of graphite powder, 2.5 g of $K_2S_2O_8$, and 2.5 g of P_2O_5 were added into 12 mL concentrated H_2SO_4 and then kept at 80 °C for 4.5 h. The product was dried in air at ambient temperature overnight, after being washed with deionized water until pH neutral. Pretreated graphite powder was put into 0 °C concentrated H_2SO_4 (120 mL). Then, 15 g of $KMnO_4$ was added gradually under stirring, and the temperature of the mixture was kept to be below 20 °C by cooling. Successively, the mixture was stirred at 35 °C for 2 h, and then diluted with deionized water (DW). After that, 20 mL of 30% H_2O_2 was added to the mixture, and filtered and washed with 1:10 HCl to remove metal ions followed by DW to remove the acid. The resulting solid was dried in air and diluted to make a graphite oxide dispersion. Finally, it was purified by dialysis for 1 week to remove the remaining metal species. Exfoliation was performed by sonicating graphite oxide dispersion under ambient condition for 20 min. CGO was prepared from GO through reacting with chloroacetic acid under strong alkaline condition according to procedure reported previously [29]. Specifically, 50 mL of GO aqueous suspension with concentration of 2.0 mg mL^{-1} was bath sonicated for 30 min to obtain a clear solution. Then 6.0 g of NaOH and 5.0 g of chloroacetic acid were added into the GO suspension under stirring and ultrasonication. After that, the mixture reacted by bath sonication for 3 h to obtain CGO. The CGO suspension was neutralized, and purified by repeated rinse with DW and filtration to remove excess reactant, followed by drying at 50 °C in vacuum oven for 24 h.

Fabrication of electrodes

CGO-PEDOT and GO-PEDOT electrodes were prepared via in situ electrochemical polymerization in an aqueous deposition bath containing 0.01 M EDOT monomer and 2 mg mL^{-1} CGO or GO, respectively. Prior to use, the deposition bath was dispersed adequately under ultrasonication. A typical three-electrode cell, equipped with a graphite foil with 1 cm × 1 cm of conductive area that serves as the working electrode, a platinum foil counter electrode, and a saturated calomel reference electrode (SCE), was used for electropolymerization, which was carried out with a constant low current density of 1 mA cm^{-2} for 30 min. As-prepared electrodes were rinsed with DW to remove monomer and oligomer

residues. For comparison, PEDOT electrodes were fabricated with the same procedure in an aqueous bath containing 0.01 M EDOT monomer and 0.01 M sodium dodecyl benzene sulfonate. The mass and thickness of deposits were determined by measuring the discrepancy of graphite foil before and after loading of electroactive substances, using a Mettler-Toledo microbalance with an accuracy of 10 μg and a Syntek thickness gauge with an accuracy of 1 μm, respectively.

Material characterizations

UV–Vis absorption spectra were recorded with Hitachi U-3900 spectrophotometer using quartz cuvette with 1-cm optical path. Water contact angle was measured by a Krüss DSA 100 drop shape analyzer. XPS was recorded using Thermo ESCALAB 250 X-ray photoelectron spectrometer. The XPS spectra were fitted by XPS Peak software, and Gaussian curves were fitted to the measured data. FTIR spectra and XRD patterns were acquired with Bruker Tensor 27 FTIR spectrometer and Rigaku Ultima IV X-ray diffractometer, respectively. Morphologies of electrode materials were examined by a JEOL JSM-6701F field emission SEM and a high-resolution JEOL JEM-2100 TEM. EDS patterns were obtained using a Hitachi S-4800 SEM equipped with an X-ray energy-dispersive spectrometer. For FTIR, XRD, and TEM characterizations, samples were scraped from deposit coated conducting glasses to avoid scraping off graphite.

Electrochemical measurements

Electrochemical capacitive properties of the electrodes were measured with a two-electrode cell, constructed by assembling two pieces of identical electrodes with a sandwiched filter paper soaked with 1.0 M KCl aqueous electrolyte as the separator. CV, GCD, and EIS measurements were conducted on a Chenhua CHI 660E electrochemical workstation. EIS were performed with a sinusoidal signal of 5 mV referring to the open-circuit potential, over the frequency range from 100 kHz to 0.01 Hz.

Results and discussion

Characterizations

Figure 2a shows the UV–Vis spectra of GO and CGO. Both samples present a strong characteristic peak at 230 nm due to π–π^* transition of aromatic C–C bonds, as well as a shoulder peak at 300 nm caused by n-π^* transition of C=O bonds [30]. The inset of Fig. 2a indicates that CGO (40.7°) has a smaller contact angle than GO (56.2°). It is thus favorable for the access of electrolyte in CGO-based electrode materials, owing to better hydrophilicity. Figure 2b shows homogenous brown–yellow GO and black CGO colloidal dispersion in DW, respectively. Both exhibit Tyndall effect as compared to DW, which facilitates the preparation of GO or CGO composites with PEDOT in homogenous colloidal deposition bath via electrochemical polymerization. Color change from GO to CGO also leads to an increase in UV–Vis absorbance (Fig. 2a). This is attributed to the restoration of electronic conjugation within graphene plane, due to the opening of epoxide rings and hydrolysis of esters on GO during carboxylation [31].

Figure 2c shows the high-resolution C 1s XPS spectra of GO and CGO. Both are deconvoluted into five peaks at 284.4, 285, 286.6, 287.1, and 288.5 eV, corresponding to C=C bonds formed by sp^2 carbon, C–C bonds formed by sp^3 carbon, C–O, C=O, and O–C=O, respectively. Based on peak area, the proportion of C–O in various C species for GO and CGO are calculated to decrease from 43.6 to 29.2%, while that of O–C=O increases from 8.5 to 14.0%. These numbers indicate that hydroxyl and epoxide groups on the basal plane of GO were partially converted into carboxyl group through carboxylation.

FTIR spectra of GO, CGO, PEDOT, GO-PEDOT, and CGO-PEDOT are presented in Fig. 3a. For GO, main bands (and assignments) are as follows [32–34]: C=O stretching at 1729 cm^{-1}, aromatic C=C stretching or absorbed water at 1620 cm^{-1}, O–H deformation at 1398 cm^{-1}, C–OH stretching at 1227 cm^{-1}, and C–O stretching of alkoxy group at 1060 cm^{-1}. The vibration at 852 cm^{-1} is attributed to epoxide group. The spectrum of CGO shows the same set of peaks, indicating that it contains the same functional groups as GO. Nevertheless, compared to GO, the C=O stretching of carboxyl group at 1729 cm^{-1} for CGO is strengthened, while peaks at 1227 originating from C–OH and 852 cm^{-1} ascribed to C–O–C group are

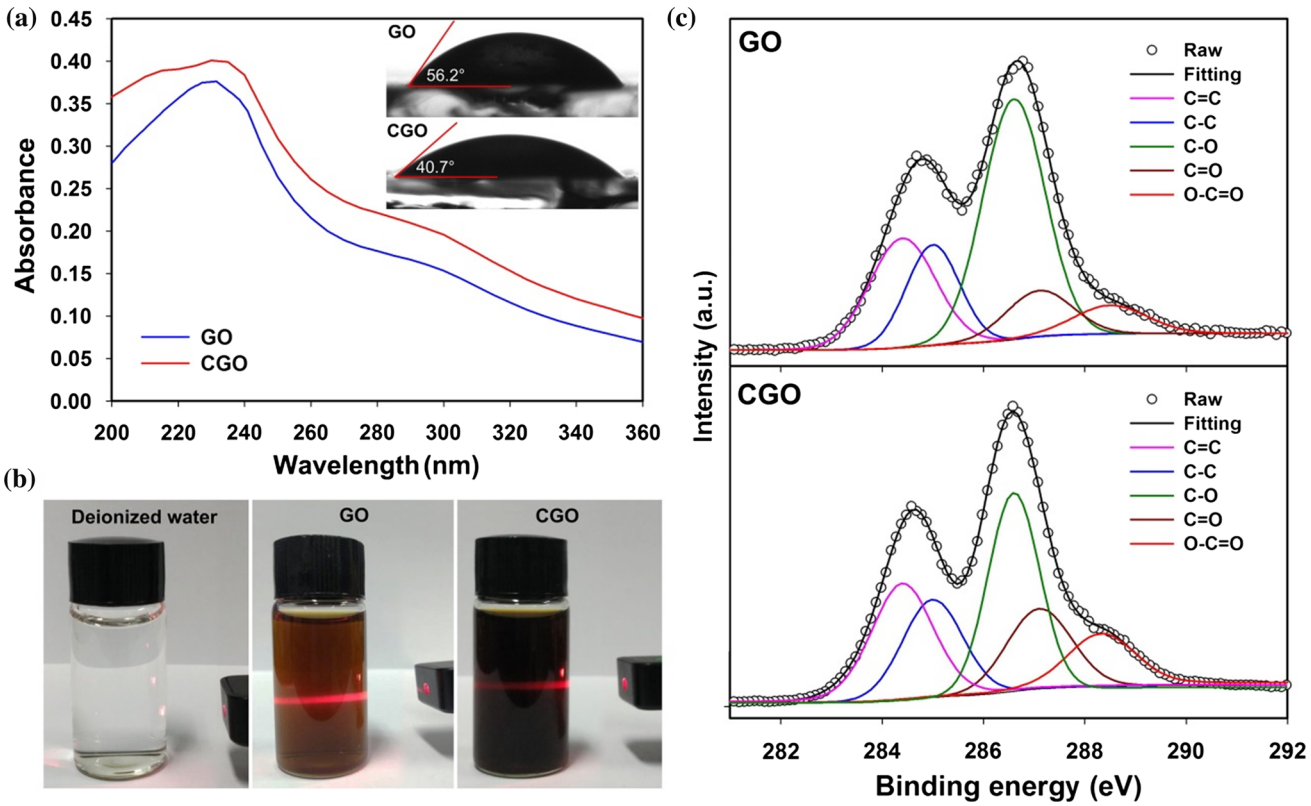

Figure 2 **a** UV–Vis spectra of 0.01 mg mL^{-1} GO and CGO aqueous suspension. The inset shows water contact angle of GO and CGO films spread evenly on glass. **b** Tyndall scattering effect of 1 mg mL^{-1} of GO and CGO dispersed in deionized water. **c** The C 1s XPS spectra of GO and CGO.

weakened. These differences further suggest that hydroxyl and epoxide groups in GO were partially transformed into carboxyl groups through carboxylation.

For PEDOT, vibration peaks at 1348 and 1518 cm^{-1} are due to C–C and C=C stretching in thiophene ring, respectively. Absorptions at 1056, 1088, 1144, and 1201 cm^{-1} are attributed to stretching in ethylenedioxy ring, the peak at 926 cm^{-1} is associated to deformation of ethylenedioxy ring, and peaks at 691, 838, and 980 cm^{-1} are due to C–S bond in thiophene ring [35, 36]. These peaks are also observed in the GO-PEDOT and CGO-PEDOT composites, confirming the presence of PEDOT in the composites. However, using PEDOT as reference, the difference for GO-PEDOT and CGO-PEDOT composites is that absorption peak at 1348 cm^{-1} (due to C–C stretching of thiophene ring of PEDOT) is downshifted to 1329 cm^{-1}. This shift is associated to π–π interaction and hydrogen bonding between thiophene rings of PEDOT and GO or CGO nanosheet layers, as well as electrostatic interaction between cationic PEDOT and anionic GO or CGO [23]. In the two types of composites, unobvious detection for peaks of GO and CGO is probably because their information overlaps with that of PEDOT coating, or becomes too weak relative to that of PEDOT [37].

GO, CGO, PEDOT, GO-PEDOT, and CGO-PEDOT composites were further characterized by XRD. As shown in Fig. 3b, pristine graphite has an intense sharp peak at $2\theta = 26.6°$, the interlayer distance (d-spacing) of which is calculated to be 0.335 nm using the Bragg equation. In contrast, GO and CGO show sharp peaks at $2\theta = 11.4°$ and 11.8°, respectively, corresponding to d-spacings of 0.78 and 0.75 nm. The d-spacing of GO nanosheets slightly decreases owing to carboxylation treatment. Compared to graphite, enlarged d-spacing for GO and CGO is ascribed to the introduction of oxygenated functional groups and intercalated water molecules between layers [38]. For PEDOT, a broad diffraction peak is present at $2\theta = 26.0°$, indicative of amorphous nature [39]. The same peak at $2\theta = 26.0°$ is observed in both GO-PEDOT and CGO-PEDOT composites. The

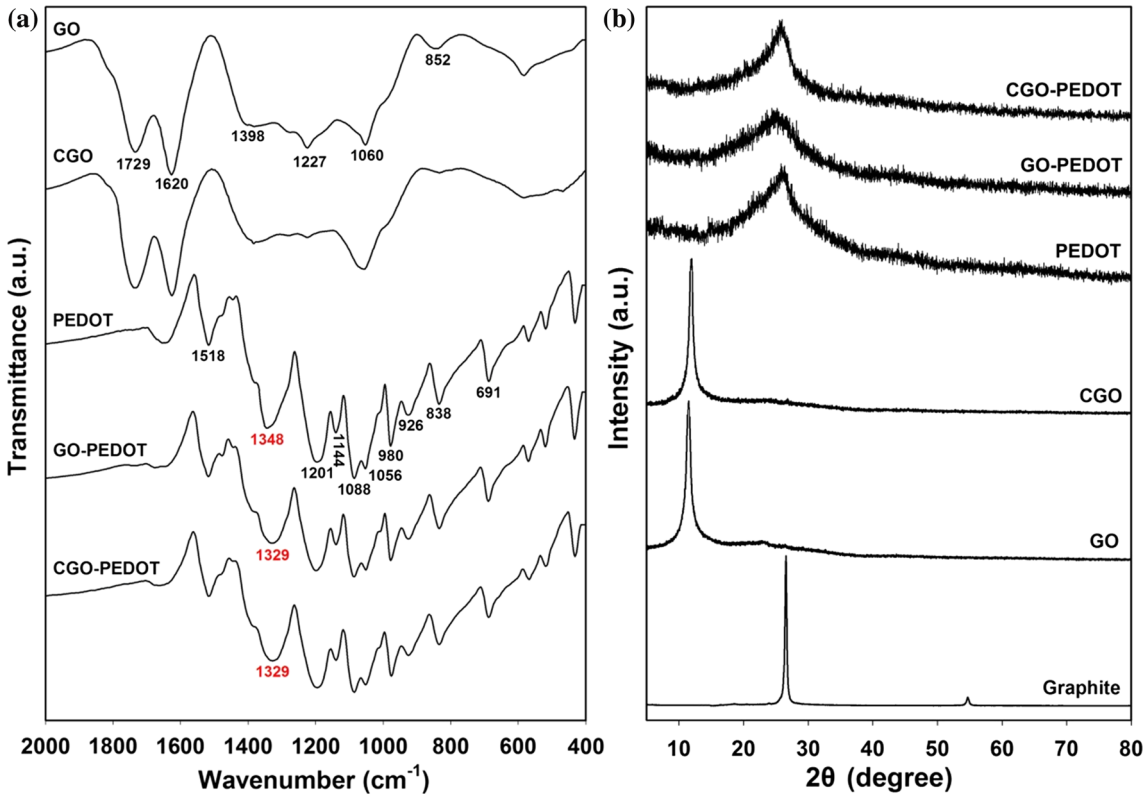

Figure 3 **a** FTIR spectra of GO, CGO, PEDOT, GO-PEDOT, and CGO-PEDOT. **b** XRD patterns of CGO-PEDOT, GO-PEDOT, PEDOT, CGO, GO, and graphite.

disappearance of peaks associated to GO or CGO is probably related to complete coating of PEDOT between layered GO or CGO nanosheets, which results in increasing d-spacing [40].

Surface morphology of electroactive materials has a large effect on their electrochemical properties. Figure 4a shows the SEM images of PEDOT, GO-PEDOT, and CGO-PEDOT. Their mass per unit area is measured to be 1.25, 1.20, and 1.18 mg cm^{-2}, and their thickness is 16, 20, and 21 μm, respectively. PEDOT contains numerous dense particles that aggregate into cauliflower-like morphology of a few micrometers in diameter. The compact microstructure is unfavorable for the access of electrolyte. In contrast, GO-PEDOT composite shows distinctly different morphology after GO is incorporated into PEDOT matrix. Curly morphology of two-dimensional GO nanosheets that interconnect with each other is observed clearly, and compact structures of PEDOT disappear. This is because PEDOT as coating covers GO nanosheets during electropolymerization, and GO sheets, due to their large surface area, lead to dispersed distribution of PEDOT. Such loose and dispersed structures can shorten the diffusion path of electrolyte, as well as increase the contact between electrolyte and PEDOT with high pseudocapacitance, thereby facilitating the utilization of more PEDOT for charge storage. CGO-PEDOT composite has similar morphology with GO-PEDOT, that is, PEDOT coating is dispersedly distributed on CGO sheets. The difference is that curly sheet-like morphology of CGO-PEDOT becomes not so obvious relative to that of GO-PEDOT, which is ascribed to the fact that more PEDOT is introduced as coating, covering the curly morphology of CGO nanosheets.

EDS characterizations were performed to determinate elementary composition of the composites. As listed in Fig. 4b, CGO-PEDOT has an increased C/O atom ratio, owing to the introduction of more PEDOT. Atom amount of S originating from PEDOT increases from 2.87% for GO-PEDOT to 4.32% for CGO-PEDOT. Figure 4c shows the TEM images, revealing morphological details for the as-prepared composites. Compared to GO-PEDOT, CGO-PEDOT has more dark area on its nanosheets due to more PEDOT coating. Although both of them exhibit

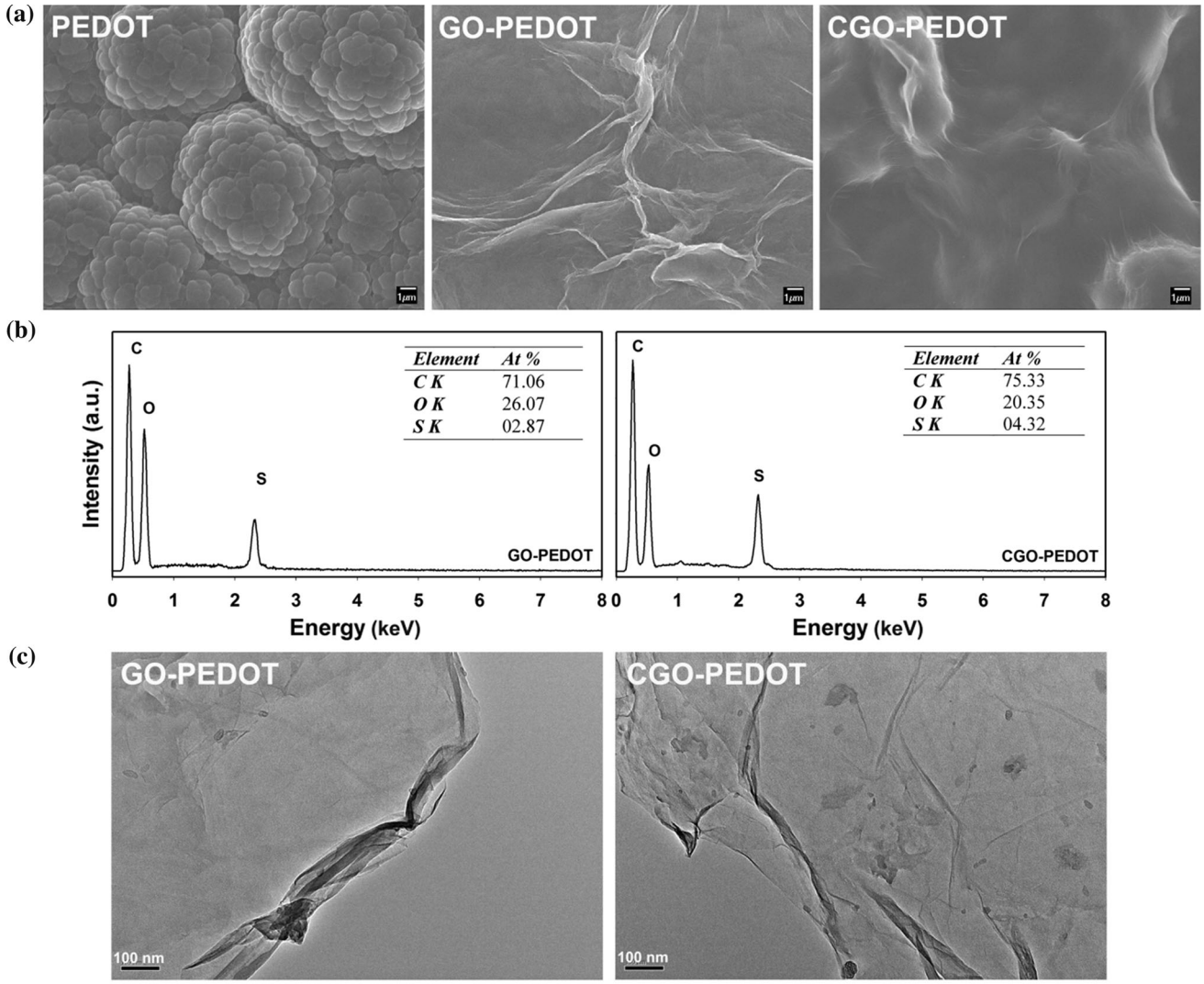

Figure 4 **a** SEM images of PEDOT, GO-PEDOT, and CGO-PEDOT composites. **b** EDS patterns of GO-PEDOT and CGO-PEDOT. **c** TEM images of GO-PEDOT and CGO-PEDOT.

wrinkled paper-like structures, GO-PEDOT has obvious curly edges with respect to CGO-PEDOT. In line with SEM and EDS, this is because more PEDOT coating is introduced in CGO-PEDOT composite, which smoothens the curly edges.

Electrochemical properties

Figure 5a shows the CV curves at the scan rate of 10 mV s^{-1} for PEDOT, GO-PEDOT, and CGO-PEDOT electrodes. CV curve of PEDOT electrodes deviates from rectangle, indicative of unsatisfactory supercapacitive nature. In contrast, both GO-PEDOT and CGO-PEDOT electrodes show rectangular shape, and in particular the curve for CGO-PEDOT electrodes is nearly perfect. Furthermore, the rectangular CV curves have symmetric *I*–*E* responses up to 100 mV s^{-1} (Fig. 5b), and the current density increases persistently at higher scan rate, demonstrating that CGO-PEDOT electrodes have superior rate capability, a key specification for supercapacitors.

Electrochemical capacitive properties of electrodes may be assessed based on areal specific capacitance, a better performance indicator when supercapacitors are used for small-scale electronics and energy storage of stationary devices [41–43]. Areal specific capacitance (C_S) in F cm^{-2} of electrodes is calculated from the CV curves by the following equation:

$$C_S = \left(\int I dV\right)/(S \times \Delta V \times v), \quad (1)$$

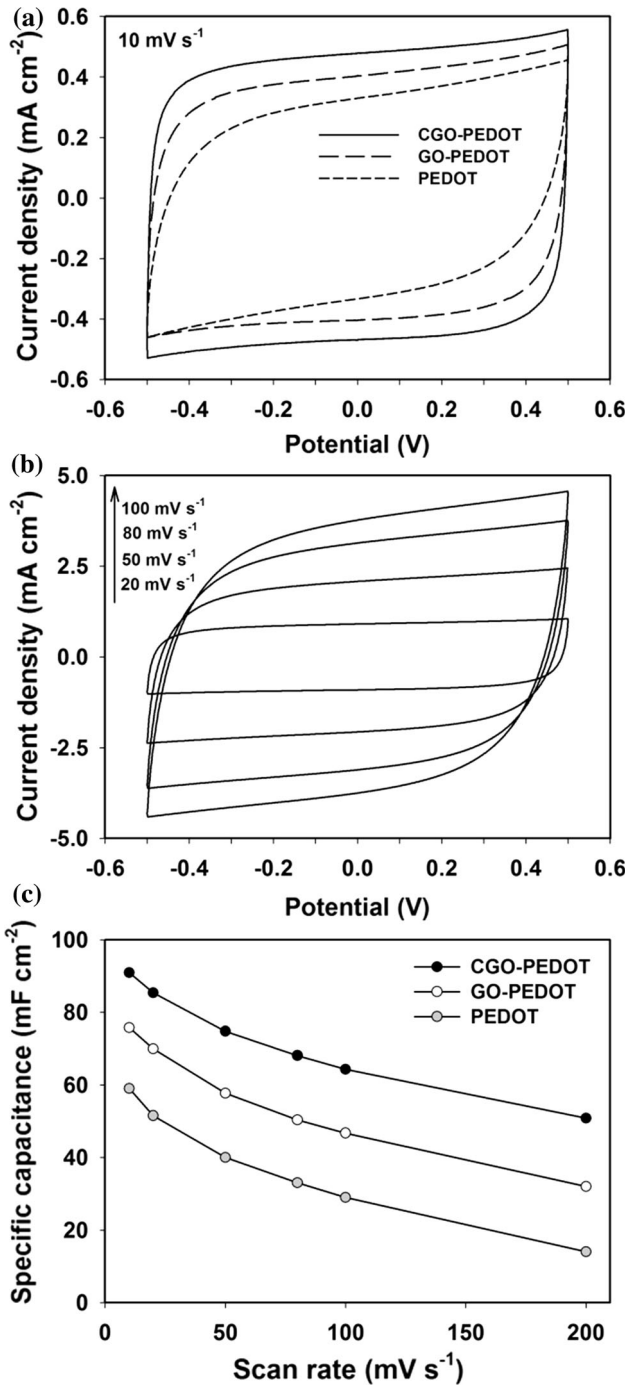

Figure 5 **a** CV curves at the scan rate of 10 mV s^{-1} for PEDOT, GO-PEDOT, and CGO-PEDOT composite electrodes. **b** CV curves at the scan rate ranging from 20 to 100 mV s^{-1} for CGO-PEDOT composite electrode. **c** Relationship of areal specific capacitance with CV scan rate for PEDOT, GO-PEDOT, and CGO-PEDOT electrodes.

where $\int I\,dV$ represents the integrated area of the CV curve; S is the geometric surface area of electrode in cm^2; ΔV the scanning potential window in V; and v the scan rate in V s^{-1}. Figure 5c shows that CGO-PEDOT electrodes have the highest specific capacitance at all scan rates, while PEDOT electrodes have the lowest. CGO-PEDOT electrodes achieve a specific capacitance of 90.9 mF cm^{-2} at 10 mV s^{-1}, which is 20.2 and 53.8% higher than those for GO-PEDOT (75.6 mF cm^{-2}) and PEDOT (59.1 mF cm^{-2}), respectively. Compared to PEDOT, the promoted supercapacitive performance for GO-PEDOT and CGO-PEDOT can be attributed to three factors: (1) The introduction of GO and CGO nanosheets increases the specific surface area of electrodes; (2) unlike the aggregated morphology of pure PEDOT, GO, and CGO nanosheets improve the dispersion of PEDOT as coating, allowing more PEDOT to be utilized for electrochemical energy storage; (3) hydrophilic GO and CGO nanosheets boost the wettability of composite electrodes, enabling aqueous electrolyte to access easily. Compared with GO-PEDOT, the enhanced capacitive performance for CGO-PEDOT is related to more polymerized PEDOT and dispersed distribution.

Supercapacitive performances of GO-PEDOT and CGO-PEDOT composites were further compared by GCD tests. Figure 6a shows the GCD curves at 0.2 mA cm^{-2} for the two types of PEDOT composite electrodes. Both curves exhibit triangle shape, and yet CGO-PEDOT electrodes have longer discharge time. The ratio of discharge time (t_d) to charge time (t_c) is defined as the columbic efficiency (η). The η at 0.2 mA cm^{-2} for CGO-PEDOT electrodes is 97.0%, which is higher than 95.7% for GO-PEDOT electrodes. Figure 6b shows the GCD curves at higher current densities. The CGO-PEDOT electrodes have lower IR drop relative to GO-PEDOT electrodes, indicating that supercapacitor cell assembled with CGO-PEDOT electrodes has a smaller internal resistance. This is important for energy-storing devices, because it will save energy by decreasing the production of unwanted heat during charging/discharging [44].

The C_S (F cm^{-2}) of electrodes can be obtained according to GCD curves through Eq. (2):

$$C_S = (2 \times I \times t)/(S \times \Delta V), \quad (2)$$

here I (A) is the discharge current, t (s) the discharge time, S (cm^{-2}) the geometric surface area of electrode, and ΔV (V) the potential window tested. In line with the CV results, Fig. 6c suggests that CGO-PEDOT

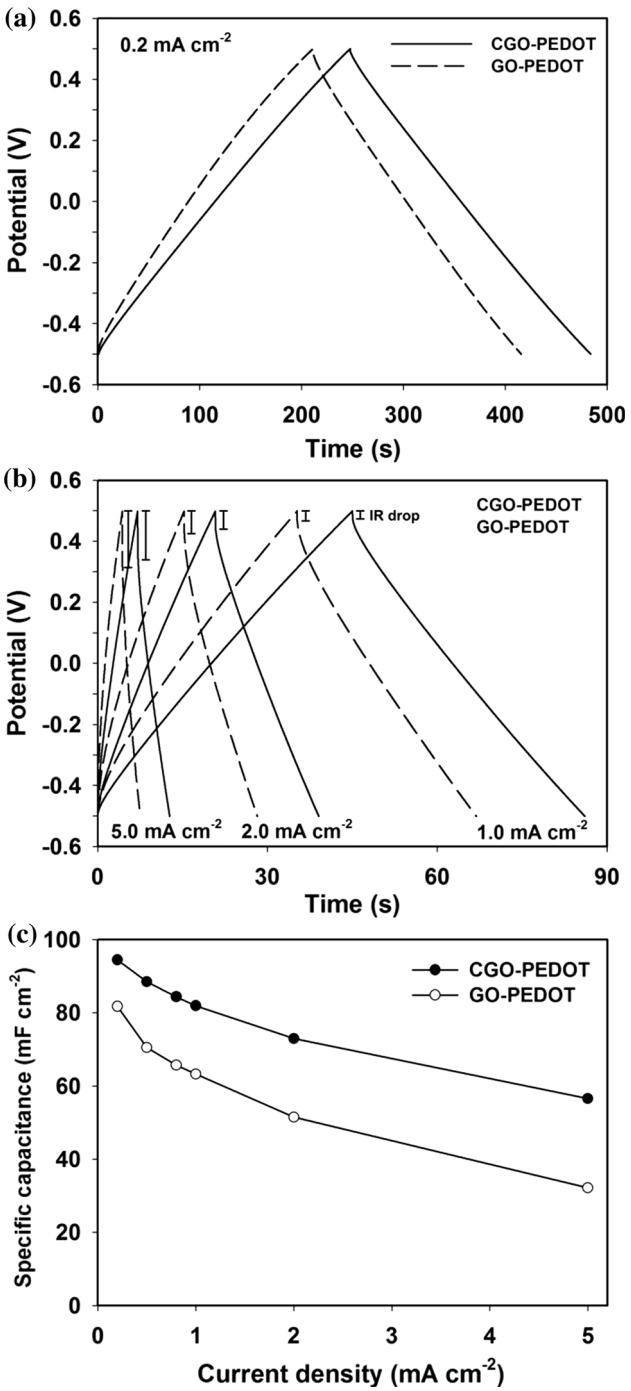

Figure 6 GCD curves at current density of **a** 0.2 and **b** 1.0, 2.0, and 5.0 mA cm^{-2}. Shown in **c** are plots of specific capacitance vs. GCD current density for GO-PEDOT and CGO-PEDOT electrodes.

electrodes have higher C_S than GO-PEDOT electrodes at current densities ranging from 0.2 to 5 mA cm^{-2}. Thereinto, CGO-PEDOT electrodes deliver a high specific capacitance of 94.4 mF cm^{-2} at 0.2 mA cm^{-2}, which is to be compared to those of recently reported CP-based electrode materials: 77.0 mF cm^{-2} at 1 mA cm^{-2} for polyoxometalate (POM)-doped PPy nanopillar [45], 40.0 mF cm^{-2} at 0.45 mA cm^{-2} for H-TiO_2/Prussian blue/PEDOT [46], 43.75 mF cm^{-2} at 0.2 mA cm^{-2} for rGO/PEDOT [47], 67.2 mF cm^{-2} at 0.05 mA cm^{-2} for 3D porous graphene/PANI composite [48], and 6.3 mF cm^{-2} at 0.16 mA cm^{-2} for graphite oxide/PANI composite [49]. In addition, the C_S of CGO-PEDOT electrodes shows a smoother decline compared to GO-PEDOT electrodes with the increase in GCD current density. When the current density is increased from 0.2 to 5.0 mA cm^{-2}, CGO-PEDOT electrodes retain 59.9% of initial capacitance, while GO-PEDOT electrodes only maintain 39.4%, indicating that the rate capability is remarkably boosted after carboxylation of GO.

To further confirm the advantages of CGO-PEDOT composite over GO-PEDOT composite as electrode material for supercapacitors, electrochemical properties were characterized by EIS measurements. Figure 7a shows the EIS complex plane plots of CGO-PEDOT and GO-PEDOT electrodes. Capacitive character is observed for both types of electrodes, because both of them display a vertical trend for impedance plots at low frequencies [50]. The difference is that the straight line of CGO-PEDOT in low-frequency region leans more toward the imaginary axis, indicating better capacitive behavior as compared to GO-PEDOT. Equivalent series resistance (ESR), a key specification to electrochemical energy-storing devices, can be determined by the intercept at x axis in EIS complex plane plots. It is associated with the electrolyte solution resistance, intrinsic resistance of active materials, and interfacial contact resistance between active materials and current collectors [51]. The inset of Fig. 7a shows that CGO-PEDOT electrodes have smaller ESR.

Knee frequency (f_{knee}) is the maximum frequency at which predominant capacitive behavior is maintained, determined by the crossing of Warburg-type line (inclined 45°) and low-frequency vertical line. We can see from the inset of Fig. 7a that CGO-PEDOT has higher f_{knee} (2.6 Hz) than GO-PEDOT (1.2 Hz), indicating that CGO-PEDOT electrodes have faster charge transfer and ion diffusion of electrolyte [52, 53]. Further, the C_S (F cm^{-2}) can be obtained from EIS plots, which is calculated from Eq. (3):

$$C_S = -1/(\pi S f Z'') \quad (3)$$

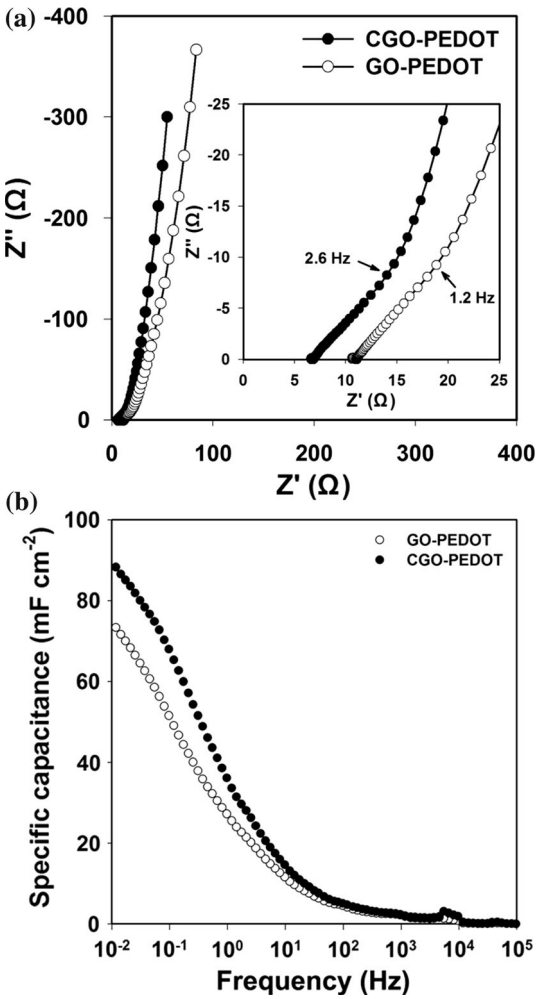

Figure 7 **a** EIS complex plane plots of GO-PEDOT and CGO-PEDOT composite electrodes. The insert shows EIS plots at high frequencies. **b** Relationship of specific capacitance with EIS scanning frequency for GO-PEDOT and CGO-PEDOT electrodes.

where S is the geometric surface area of electrode, f the scanning frequency in Hz, and Z″ the imaginary part of EIS plots in Ω. In line with CV and GCD results, the CGO-PEDOT electrodes exhibit larger specific capacitance in the whole frequency region (Fig. 7b). The enhanced supercapacitive properties for CGO-PEDOT composite are due to the fact that more PEDOT with superior pseudocapacitive properties is introduced into the composite, and PEDOT is more dispersedly distributed on CGO nanosheets.

Ragone plot and cycling stability

Energy density and power density of electrodes are two key metrics for their performances. Areal specific energy density (E in Wh cm^{-2}) and power density (P in W cm^{-2}) of CGO-PEDOT and GO-PEDOT electrodes depicted in the Ragone plots (Fig. 8a) are calculated according to Eqs. (4) and (5), respectively [49, 54].

$$E = \frac{\frac{1}{2}C_S \Delta V^2}{3600} \tag{4}$$

$$P = \frac{3600E}{t} \tag{5}$$

where C_S is the areal specific capacitance in F cm^{-2}, ΔV the potential window excluding IR drop in V, and t the discharge time in s. 3600 is for unit conversion from second to hour. CGO-PEDOT electrodes have higher energy and power densities, achieving a maximum power density of 6.6 mW cm^{-2} and the highest energy density of 13.1 μWh cm^{-2}, which are also higher than those of recently reported CP-based supercapacitor electrodes, such as PEDOT/GO [23], PANI/graphite oxide [49], PEDOT/SDS-GO [54], and PPy-carbon paper [55]. Note that the Ragone plot of CGO-PEDOT electrodes has a trend of smooth

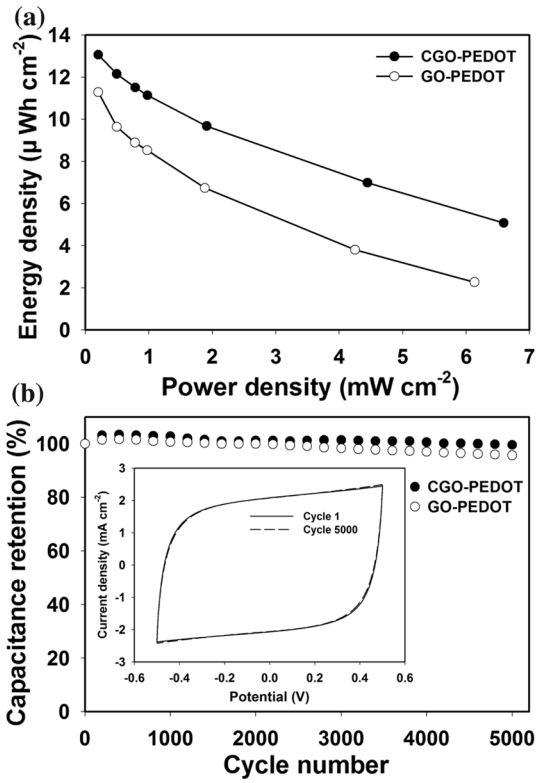

Figure 8 **a** Ragone plots of GO-PEDOT and CGO-PEDOT electrodes. **b** Plots of capacitance retention as a function of cycle number for GO-PEDOT and CGO-PEDOT electrodes. The inset in **b** shows CV curves at 50 mV s^{-1} of CGO-PEDOT electrodes at cycle 1 and cycle 5000.

decline relative to that of GO-PEDOT electrodes, further indicating superior rate capability of the former electrodes.

Figure 8b shows the variation of capacitance retention of CGO-PEDOT and GO-PEDOT electrodes, suffering from 5000 CV cycles at the scan rate of 50 mV s^{-1}. Stability tests reveal an initial increase in specific capacitance for the two types of electrodes. Hydrophilic GO and CGO nanosheets in the composites induce more electroactive surface area with the surface gradual wetting during cycling tests [56, 57]. After 5000 cycles, CGO-PEDOT and GO-PEDOT electrodes retain 99.6 and 95.7% of initial capacitance, respectively. In particular, CGO-PEDOT composite retains nearly unchanged CV curves before and after cycling tests (inset of Fig. 8b), indicative of excellent cycling stability. The higher stability for CGO-PEDOT electrodes is associated with relatively dispersed PEDOT coating. Besides, better hydrophilicity of CGO improves the wettability of composite to electrolyte during cycling.

Conclusions

We have demonstrated herein a composite electrode material, that is, carboxylated graphene oxide-doped poly(3,4-ethylenedioxythiophene), or CGO-PEDOT for short, for boosted electrochemical properties. GO has suffered from a carboxylation treatment to convert hydroxyl and epoxy groups on its basal planes of nanosheets to carboxyl group. CGO provides more active sites for dispersion and polymerization of PEDOT, due to more carboxyl groups being distributed on both edges and basal planes of nanosheets. The as-prepared CGO-PEDOT composite electrodes show satisfactory supercapacitive performances, such as good rate capability, high areal specific capacitance (90.9 mF cm^{-2} at 10 mV s^{-1}), and excellent cycling stability (retaining 99.6% of initial capacitance for 5000 cycles), which make the CGO-PEDOT composite competitive for high-performance supercapacitor applications. The present system is anticipated to serve as a new platform for the development of composite electrode materials based on CGO-conducting polymers in electrochemical energy storage.

Acknowledgements

This work was supported by the National Natural Science Foundation of China (21601113 and 21573138), Natural Science Foundation of Shanxi Province (2015021079), Scientific and Technological Innovation Programs of Higher Education Institutions in Shanxi (2017112), and China Postdoctoral Science Foundation (2015M571283). H.J.Z. also gratefully acknowledges support from the Sanjin Scholar Distinguished Professors Program.

References

[1] Cheng C, Li S, Thomas A, Kotov NA, Haag R (2017) Functional graphene nanomaterials based architectures: biointeractions, fabrications, and emerging biological applications. Chem Rev 117:1826–1914

[2] Khan U, Kim TH, Ryu H, Seung W, Kim SW (2017) Graphene tribotronics for electronic skin and touch screen applications. Adv Mater 29:1603544

[3] Wu J, Wang JY, Pan DF, Li YC, Jiang CH, Li YB, Jin C, Wang K, Song FQ, Wang GH, Zhang H, Wan JG (2017) Synchronous growth of high-quality bilayer bernal graphene: from hexagonal single-crystal domains to wafer-scale homogeneous films. Adv Funct Mater 27:1605927

[4] Xie QX, Zhao P, Wu SH, Zhang YF (2017) Flexible carbon@graphene composite cloth for advanced lithium-sulfur batteries and supercapacitors with enhanced energy storage capability. J Mater Sci 52:13478–13489. https://doi.org/10.1007/s10853-017-1451-5

[5] Wang SL, Liu NS, Su J, Li LY, Long F, Zou ZG, Jiang XL, Gao YH (2017) Highly stretchable and self-healable supercapacitor with reduced graphene oxide based fiber springs. ACS Nano 11:2066–2074

[6] Zhang LF, Wang WJ, Cheng J, Shi YH, Zhang Q, Dou P, Xu XH (2018) Skeleton networks of graphene wrapped double-layered polypyrrole/polyaniline nanotubes for supercapacitor applications. J Mater Sci 53:787–798. https://doi.org/10.1007/s10853-017-1543-2

[7] Ke QQ, Guan C, Zhang X, Zheng MR, Zhang YW, Cai YQ, Zhang H, Wang J (2017) Surface-charge-mediated formation of H-TiO_2@$Ni(OH)_2$ heterostructures for high-performance supercapacitors. Adv Mater 29:1604164

[8] Guo HY, Yeh MH, Lai YC, Zi YL, Wu CS, Wen Z, Hu CG, Wang ZL (2016) All-in-one shape-adaptive self-charging

power package for wearable electronics. ACS Nano 10:10580–10588

[9] Liu L, Wang Y, Meng QH, Cao B (2017) A novel hierarchical graphene/polyaniline hollow microsphere as electrode material for supercapacitor applications. J Mater Sci 52:7969–7983. https://doi.org/10.1007/s10853-017-1000-2

[10] Panmand RP, Patil P, Sethi Y, Kadam SR, Kulkarni MV, Gosavi SW, Munirathnam NR, Kale BB (2017) Unique perforated graphene derived from Bougainvillea flowers for high-power supercapacitors: a green approach. Nanoscale 9:4801–4809

[11] Wang HL, Hao QL, Yang XJ, Lu LD, Wang X (2010) Effect of graphene oxide on the properties of its composite with polyaniline. ACS Appl Mater Interfaces 2:821–828

[12] Li NT, Tang SC, Dai YM, Meng XK (2014) The synthesis of graphene oxide nanostructures for supercapacitors: a simple route. J Mater Sci 49:2802–2809. https://doi.org/10.1007/s10853-013-7986-1

[13] De B, Kuila T, Kim NH, Lee JH (2017) Carbon dot stabilized copper sulphide nanoparticles decorated graphene oxide hydrogel for high performance asymmetric supercapacitor. Carbon 122:247–257

[14] Wang M, Han XX, Zhao Y, Li JJ, Ju P, Hao ZM (2017) Tuning size of MoS_2 in MoS_2/graphene oxide heterostructures for enhanced photocatalytic hydrogen evolution. J Mater Sci. https://doi.org/10.1007/s10853-017-1745-7

[15] Anothumakkool B, Soni R, Bhange SN, Kurungot S (2015) Novel scalable synthesis of highly conducting and robust PEDOT paper for a high performance flexible solid supercapacitor. Energy Environ Sci 8:1339–1347

[16] D'Arcy JM, El-Kady MF, Khine PP, Zhang LH, Lee SH, Davis NR, Liu DS, Yeung MT, Kim SY, Turner CL, Lech AT, Hammond PT, Kaner RB (2014) Vapor-phase polymerization of nanofibrillar poly(3,4-ethylenedioxythiophene) for supercapacitors. ACS Nano 8:1500–1510

[17] Perez-Madrigal MM, Estrany F, Armelin E, Diaz DD, Aleman C (2016) Towards sustainable solid-state supercapacitors: electroactive conducting polymers combined with biohydrogels. J Mater Chem A 4:1792–1805

[18] Liu YQ, Weng B, Razal JM, Xu Q, Zhao C, Hou YY, Seyedin S, Jalili R, Wallace GG, Chen J (2015) High-performance flexible all-solid-state supercapacitor from large free-standing graphene-PEDOT/PSS films. Sci Rep 5:17045

[19] Zhao ZH, Richardson GF, Meng QS, Zhu SM, Kuan HC, Ma J (2016) PEDOT-based composites as electrode materials for supercapacitors. Nanotechnology 27:042001

[20] Azman NHN, Lim HN, Sulaiman Y (2016) Effect of electropolymerization potential on the preparation of PEDOT/-graphene oxide hybrid material for supercapacitor application. Electrochim Acta 188:785–792

[21] Wang MC, Jamal R, Wang YJ, Yang L, Liu FF, Abdiryim T (2015) Functionalization of graphene oxide and its composite with poly(3,4-ethylenedioxythiophene) as electrode material for supercapacitors. Nanoscale Res Lett 10:370

[22] Abidin SNJSZ, Azman NHN, Kulandaivalu S, Sulaiman Y (2017) Poly(3,4-ethylenedioxythiophene) doped with carbon materials for high-performance supercapacitor: a comparison study. J Nanomater 2017:5798614

[23] Zhou HH, Zhai HJ, Han GY (2016) Adjust the electrochemical performances of graphene oxide nanosheets-loaded poly(3,4-ethylenedioxythiophene) composites for supercapacitors with ultralong cycle life. J Mater Sci Mater Electron 27:2773–2782

[24] Islam MM, Chidembo AT, Aboutalebi SH, Cardillo D, Liu HK, Konstantinov K, Dou SX (2014) Liquid crystalline graphene oxide/PEDOT:PSS self-assembled 3D architecture for binder-free supercapacitor electrodes. Front Energy Res 2:31

[25] Osterholm A, Lindfors T, Kauppila J, Damlin P, Kvarnstrom C (2012) Electrochemical incorporation of graphene oxide into conducting polymer films. Electrochim Acta 83:463–470

[26] Park S, Ruoff RS (2009) Chemical methods for the production of graphenes. Nat Nanotechnol 4:217–224

[27] Hummers WS, Offeman RE, Hummers WS, Offeman RE (1958) Preparation of graphitic oxide. J Am Chem Soc 80:1339

[28] Xu YX, Bai H, Lu GW, Li C, Shi GQ (2008) Flexible graphene films via the filtration of water-soluble noncovalent functionalized graphene sheets. J Am Chem Soc 130:5856–5857

[29] Sun XM, Liu Z, Welsher K, Robinson JT, Goodwin A, Zaric S, Dai HJ (2008) Nano-graphene oxide for cellular imaging and drug delivery. Nano Res 1:203–212

[30] Zhang K, Heo N, Shi X, Park JH (2013) Chemically modified graphene oxide-wrapped quasi-micro Ag decorated silver trimolybdate nanowires for photocatalytic applications. J Phys Chem C 117:24023–24032

[31] Imani R, Emami SH, Faghihi S (2015) Nano-graphene oxide carboxylation for efficient bioconjugation applications: a quantitative optimization approach. J Nanopart Res 17:88

[32] Pan N, Guan DB, Yang YT, Huang ZL, Wang RB, Jin YD, Xia CQ (2014) A rapid low-temperature synthetic method leading to large-scale carboxyl graphene. Chem Eng J 236:471–479

[33] Bora C, Dolui SK (2012) Fabrication of polypyrrole/graphene oxide nanocomposites by liquid/liquid interfacial polymerization and evaluation of their optical, electrical and electrochemical properties. Polymer 53:923–932

[34] Bagherzadeh M, Ghahfarokhi ZS, Yazdi EG (2016) Electrochemical and surface evaluation of the anti-corrosion properties of reduced graphene oxide. RSC Adv 6:22007–22015

[35] Yue RR, Wang HW, Bin D, Xu JK, Du YK, Lu WS, Guo J (2015) Facile one-pot synthesis of Pd-PEDOT/graphene nanocomposites with hierarchical structure and high electrocatalytic performance for ethanol oxidation. J Mater Chem A 3:1077–1088

[36] Chen Y, Xu JH, Yang YJ, Zhao YT, Yang WY, Mao XL, He X, Li SB (2016) The preparation and electrochemical properties of PEDOT:PSS/MnO_2/PEDOT ternary film and its application in flexible micro-supercapacitor. Electrochim Acta 193:199–205

[37] Han YQ, Ding B, Tong H, Zhang XG (2011) Capacitance properties of graphite oxide/poly(3,4-ethylene dioxythiophene) composites. J Appl Polym Sci 121:892–898

[38] Guo HL, Wang XF, Qian QY, Wang FB, Xia XH (2009) A green approach to the synthesis of graphene nanosheets. ACS Nano 3:2653–2659

[39] Pandey GP, Rastogi AC (2013) Synthesis and characterization of pulsed polymerized poly(3,4-ethylenedioxythiophene) electrodes for high-performance electrochemical capacitors. Electrochim Acta 87:158–168

[40] Zhu CZ, Zhai JF, Wen D, Dong SJ (2012) Graphene oxide/polypyrrole nanocomposites: one-step electrochemical doping, coating and synergistic effect for energy storage. J Mater Chem 22:6300–6306

[41] Liu JP, Jiang J, Bosman M, Fan HJ (2012) Three-dimensional tubular arrays of MnO_2–NiO nanoflakes with high areal pseudocapacitance. J Mater Chem 22:2419–2426

[42] Wu ZS, Parvez K, Li S, Yang S, Liu ZY, Liu SH, Feng XL, Muellen K (2015) Alternating stacked graphene-conducting polymer compact films with ultrahigh areal and volumetric capacitances for high-energy micro-supercapacitors. Adv Mater 27:4054–4061

[43] Zhang C, Xing J, Fan HW, Zhang WK, Liao MY, Song Y (2017) Enlarged capacitance of TiO_2 nanotube array electrodes treated by water soaking. J Mater Sci 52:3146–3152. https://doi.org/10.1007/s10853-016-0603-3

[44] Zhou HH, Zhai HJ (2016) Rapid preparation of the hybrid of MnO_2 dispersed on graphene nanosheets with enhanced supercapacitive performance. Electrochim Acta 215:339–345

[45] Yang M, Hong SB, Yoon JH, Kim DS, Jeong SW, Yoo DE, Lee TJ, Lee KG, Lee SJ, Choi BG (2016) Fabrication of flexible, redoxable, and conductive nanopillar arrays with enhanced electrochemical performance. ACS Appl Mater Interfaces 8:22220–22226

[46] Szkoda M, Trzcinski K, Rysz J, Gazda M, Siuzdak K, Lisowska-Oleksiak A (2017) Electrodes consisting of PEDOT modified by Prussian Blue analogues deposited onto titania nanotubes—their highly improved capacitance. Solid State Ionics 302:197–201

[47] Mao XL, Yang WY, He X, Chen Y, Zhao YT, Zhou YJ, Yang YJ, Xu JH (2017) The preparation and characteristic of poly(3,4-ethylenedioxythiophene)/reduced graphene oxide nanocomposite and its application for supercapacitor electrode. Mater Sci Eng B 216:16–22

[48] Zhou QQ, Li YR, Huang L, Li C, Shi GQ (2014) Three-dimensional porous graphene/polyaniline composites for high-rate electrochemical capacitors. J Mater Chem A 2:17489–17494

[49] Wei HG, Zhu JH, Wu SJ, Wei SY, Guo ZH (2013) Electrochromic polyaniline/graphite oxide nanocomposites with endured electrochemical energy storage. Polymer 54:1820–1831

[50] Peng C, Jin J, Chen GZ (2007) A comparative study on electrochemical co-deposition and capacitance of composite films of conducting polymers and carbon nanotubes. Electrochim Acta 53:525–537

[51] Wang YR, Wei HG, Wang JM, Liu JR, Guo J, Zhang X, Weeks BL, Shen TD, Wei SY, Guo ZH (2015) Electropolymerized polyaniline/manganese iron oxide hybrids with an enhanced color switching response and electrochemical energy storage. J Mater Chem A 3:20778–20790

[52] Weng Z, Su Y, Wang DW, Li F, Du JH, Cheng HM (2011) Graphene-cellulose paper flexible supercapacitors. Adv Energy Mater 1:917–922

[53] Wang X, Gao KZ, Shao ZQ, Peng XQ, Wu X, Wang FJ (2014) Layer-by-layer assembled hybrid multilayer thin film electrodes based on transparent cellulose nanofibers paper for flexible supercapacitors applications. J Power Sources 249:148–155

[54] Zhou HH, Han GY, Fu DY, Chang YZ, Xiao YM, Zhai HJ (2014) Petal-shaped poly(3,4-ethylenedioxythiophene)/sodium dodecyl sulfate-graphene oxide intercalation composites for high-performance electrochemical energy storage. J Power Sources 272:203–210

[55] Wei HG, Wang YR, Guo J, Yan XR, O'Connor R, Zhang X, Shen NZ, Weeks BL, Huang XH, Wei SY, Guo ZH (2015) Electropolymerized polypyrrole nanocoatings on carbon paper for electrochemical energy storage. Chemelectrochem 2:119–126

[56] Xu YF, Hennig I, Freyberg D, Strudwick AJ, Schwab MG, Weitz T, Cha KCP (2014) Inkjet-printed energy storage device using graphene/polyaniline inks. J Power Sources 248:483–488

[57] Qu JY, Gao F, Zhou Q, Wang ZY, Hu H, Li BB, Wan WB, Wang XZ, Qiu JS (2013) Highly atom-economic synthesis of graphene/Mn_3O_4 hybrid composites for electrochemical supercapacitors. Nanoscale 5:2999–3005